IEEE Access
Multidisciplinary | Rapid Review | Open Access Journal

Date of publication xxxx 00, 0000, date of current version xxxx 00, 0000.

Digital Object Identifier 10.1109/ACCESS.2017.Doi Number

Charging and Discharging Current Measurements and Impact of Polarization Dynamics on Electric Field Modeling in HVDC Paper-Insulated Cables

Pasquale Cambareri[1], Carlo de Falco[2], Luca Di Rienzo[1], Paolo Seri[3] and Gian Carlo Montanari[4]

[1]Dipartimento di Elettronica, Informazione e Bioingegneria, Politecnico di Milano, Milano, Italy
[2]MOX, Dipartimento di Matematica, Politecnico di Milano, Milano, Italy
[3]LIMES, Dipartimento di Ingegneria dell'Energia Elettrica e dell'Informazione, Università di Bologna, Bologna, Italy
[4]Center for Advanced Power Systems, Florida State University, Tallahassee, FL, USA

Corresponding author: Pasquale Cambareri (e-mail: pasquale.cambareri@polimi.it).

ABSTRACT Accurate modeling and simulation of electric field transients in HVDC cables is an important support to optimize insulation system design and to evaluate the influence of voltage transients and steady-state conditions on accelerated ageing mechanisms and insulation reliability. Traditionally, field models considering time-independent permittivity and conductivity are used, but this approach neglects polarization mechanisms and charge trapping-detrapping phenomena. This article includes polarization dynamics in the field model and shows that its impact on transient electric field simulations in HVDC paper-insulated cables can be significant. A method is presented to infer the model parameters from experimental polarization and depolarization current measurements.

INDEX TERMS HVDC cables, electrical insulation, dielectric polarization, electric field transient.

I. INTRODUCTION

High Voltage Direct Current (HVDC) systems constitute already an important pillar of electric power grids, and their presence is expected to grow massively in the future. A fundamental element of HVDC systems is insulation, which is the weakest component of any electric system and it must be properly managed to prevent fast ageing and premature failures. This paper focuses of HVDC cables, generally employed for long distance power transmission.

There are two major factors causing extrinsic, accelerated electrical insulation ageing under DC supply [1], that is, space charge (SC) and partial discharges (PD). The former is responsible for the distortion of the Laplacian electric field that may lead to considerable local field magnification, increasing unpredictably electrical stress and, thus, reducing life [2,3,4]. PD take place in defects distributed inside insulation and containing low-density matter. They occur when the nominal voltage in the defect is higher than the inception voltage [5,6,7], which is the minimum voltage required to trigger a PD in a defect. Their impact on ageing comes from their magnitude and repetition rate, that is, the number of discharges in the unit of time.

In order to infer intrinsic and extrinsic accelerated aging mechanism [8], accurate simulation of electric field inside insulation, both in steady state and transient conditions, is necessary. Indeed, stress magnitude and distribution may change considerably from transient conditions, when it is mostly driven by permittivity, to steady-stated DC, when it is driven by conductivity [9]. This may impact both the PD inception voltage and the cumulative (intrinsic) aging process through the change of the voltage endurance coefficient, *n*, of the life-line model [3,8]

$$L = t_0 \left(\frac{E}{ES_0} \right)^{-n}, \tag{1}$$

being E the electrical stress, L life, ES_0 the reference electric stress (generally close to the electric strength) and t_0 the relevant failure time at applied field $E = ES_0$. Equation (1)

This article has been accepted for publication in a future issue of this journal, but has not been fully edited. Content may change prior to final publication. Citation information: DOI 10.1109/ACCESS.2021.3066286, IEEE Access

provides a straight life-line in a log-log coordinate system ($\log(E)$ vs $\log(L)$).

It is noteworthy that n is higher in DC than in AC, and much lower in the presence of PD [9], thus the life reduction during transient, especially if in the presence of PD, may be not negligible compared to the design DC life conceived for pure steady-state conditions. It must be also noted that voltage (and load) transient will occur even often in DC cables, due e.g., to voltage polarity inversions that are needed to change power flow direction, cable energization, ripple and harmonics superimposed to DC.

Traditional electric field simulation approaches [2,10,11] are based on the following quasi-electrostatic model:

$$\begin{cases} \nabla \cdot (\varepsilon \boldsymbol{E}) = \rho \\ \nabla \cdot \boldsymbol{J} + \dfrac{\partial \rho}{\partial t} = 0 \\ \boldsymbol{J} = \sigma(T, |\boldsymbol{E}|)\boldsymbol{E} \end{cases} \tag{2}$$

where ρ is the charge density, ε is the constant dielectric permittivity and σ is the temperature- and field-dependent electric conductivity responsible for SC accumulation under DC excitation. This model has been used successfully to compute SC and electric field profiles in HVDC cables, but it is based on static (i.e. non time-dependent) permittivity and conductivity. Actually, they both vary with time, due to polarization mechanisms (ε) [12], and charge trapping-detrapping phenomena (σ).

The focus of the work presented in the following is, indeed, to include the polarization dynamic, that is, a time dependence of permittivity, in the electric field modelling, and show how it can impact on the simulation accuracy of electric field transients. The model parameters are derived from experimental measurements of polarization and depolarization currents performed at different field and temperatures on specimens of dielectric material.

Even though the HVDC cable insulation technology has been moving recently towards solid and homogeneous dielectrics [13,14], oil-paper and laminated insulation has been and is still used, especially at the largest values of supply voltage. Therefore, this paper deals with the mature impregnated oil-paper insulation technology. This choice is not only supported by the existence of a large number of oil-paper insulated HVDC cables installed all around the world that are experiencing operating conditions they were not designed for [15] (such as high voltage and load transient rate), but also by the availability of previous studies on the modelling of dielectric polarization mechanisms in paper-oil insulation which can be used as a reference for this investigation [16].

II. MODEL

The dielectric displacement field $\boldsymbol{D}$ is related to the electric field $\boldsymbol{E}$ via

$$\boldsymbol{D} = \varepsilon_0 \boldsymbol{E} + \boldsymbol{P}\,, \tag{3}$$

where ε_0 is the vacuum electric permittivity and $\boldsymbol{P}$ is the polarization vector. Within the theory of dielectrics [11], $\boldsymbol{P}$ can be expressed as the superposition of a certain number of polarization mechanisms that respond to the application of an electric field with different characteristic times:

$$\boldsymbol{P} = \boldsymbol{P}_\infty + \sum_{k=1}^{N} \boldsymbol{P}_k\,. \tag{4}$$

$\boldsymbol{P}_\infty$ accounts for polarization mechanisms at very high frequencies (as atomic and electronic polarization) and it is related to $\boldsymbol{E}$ by

$$\boldsymbol{P}_\infty = \varepsilon_0 \chi_\infty \boldsymbol{E}\,, \tag{5}$$

where χ_∞ is the high-frequency dielectric susceptibility.
Due to technical reasons, from DC current measurements it is not possible to retrieve information on polarization mechanisms with characteristic times lower than few seconds, so that they can be incorporated in $\boldsymbol{P}_\infty$. In this way the electric displacement field becomes

$$\boldsymbol{D} = \varepsilon_0(1+\chi_\infty)\boldsymbol{E} + \sum_{k=1}^{N} \boldsymbol{P}_k = \varepsilon_\infty \boldsymbol{E} + \sum_{k=1}^{N} \boldsymbol{P}_k\,. \tag{6}$$

For the remaining polarization processes we assume a predominant Debye-type relaxation model,

$$\frac{\partial \boldsymbol{P}_k}{\partial t} = \frac{\varepsilon_0 \chi_k \boldsymbol{E} - \boldsymbol{P}_k}{\tau_k}\,, \tag{7}$$

where χ_k is the process susceptibility and τ_k is its time constant.

The dependence on field and temperature of the electric conductivity in (2) is modelled by an empirical law derived from Arrhenius' model of chemical reaction rate [2,16,17]:

$$\sigma = \sigma_0 \exp\left(-\frac{\alpha}{T} + \beta\,|\boldsymbol{E}|\right). \tag{8}$$

The electro-quasistatic model can then be written as

$$\begin{cases} \nabla \cdot \boldsymbol{D} = \rho \\ \dfrac{\partial \boldsymbol{P}_k}{\partial t} = \dfrac{\varepsilon_0 \chi_k \boldsymbol{E} - \boldsymbol{P}_k}{\tau_k} \quad k = 1, \dots, N \\ \nabla \cdot \boldsymbol{J} + \dfrac{\partial \rho}{\partial t} = 0 \\ \boldsymbol{J} = \sigma(T, |\boldsymbol{E}|)\,\boldsymbol{E} \end{cases}, \tag{9}$$

where $\boldsymbol{D}$ is given by (6). Note that if the "slow" polarization processes are negligible, i.e.

$$|\boldsymbol{P}_\infty| \gg |\boldsymbol{P}_k| \quad \forall k, \tag{10}$$

then $\boldsymbol{D} \simeq \varepsilon_\infty \boldsymbol{E}$, the second equation in (9) becomes irrelevant and the model reduces to (2).

III. MODEL PARAMETERS DERIVATION

The model parameters are permittivity ε_∞, conductivity σ, susceptibilities χ_k and time constants τ_k. They can be inferred from conduction current measurements performed

This article has been accepted for publication in a future issue of this journal, but has not been fully edited. Content may change prior to final publication. Citation information: DOI 10.1109/ACCESS.2021.3066286, IEEE Access

on flat specimens of the material under investigation: they are energized by a step DC voltage, which is kept until the measured polarization current reaches steady state; then they are short-circuited, and the depolarization current is measured. The steady-state polarization current is used to retrieve the conductivity parameters: measurements at different temperatures and electric fields are necessary to estimate σ_0, α and β in (4). The depolarization current helps to get information on the nature of the polarization processes and of the trapping dynamic [18].

Permittivity ε_∞ can be obtained from high frequency AC measurements [12], e.g., 50 Hz for the purpose of this study. If the specimen is sufficiently thin, e.g., 1 mm or less, and it can be assumed that no space charge is accumulated within it (the electric field is below the threshold for space charge accumulation [19]), the specimen can be modelled with the equivalent circuit [16] depicted in Fig. 1.

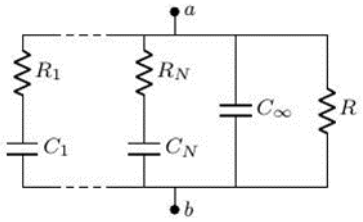

FIGURE 1. Equivalent circuit to account for polarization mechanisms in a dielectric specimen.

Assuming that the tested specimen has thickness d and area A, its equivalent circuit components are related to the model parameters as:

$$R = \frac{1}{\sigma}\frac{d}{A}, \quad C_\infty = \varepsilon_\infty \frac{A}{d}, \quad C_k = \varepsilon_0 \chi_k \frac{A}{d}, \quad R_k = \frac{\tau_k}{\varepsilon_0 \chi_k}\frac{d}{A}.$$

These relationships constitute the link between the parameters of the circuit in Fig. 1 and the ones of the differential model (9). Once the circuital parameters are identified, the corresponding differential ones are retrieved and used to perform the transient electric field simulations with (9). The flowchart in Fig. 2 helps to visualize this process.

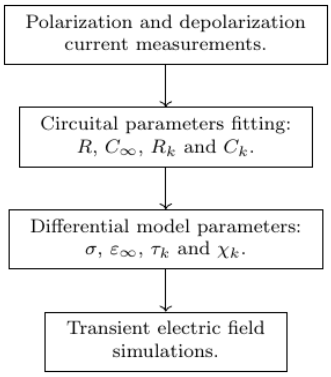

FIGURE 2. Derivation of the differential model parameters.

If a step DC voltage of amplitude V_{DC} is applied between nodes a and b in the above circuit, the resulting polarization current is, for $t > 0$,

$$i_{pol}(t) = \frac{V_{DC}}{R} + \sum_{k=1}^{N} \frac{C_k V_{DC}}{\tau_k} e^{-t/\tau_k}; \qquad (11)$$

if after a time t_{pol} the voltage is removed and the sample is short-circuited, the depolarization current in absolute value is given by

$$i_{dep}(t) = \sum_{k=1}^{N} i_k(t) = \sum_{k=1}^{N} A_k e^{-t/\tau_k} \qquad (12)$$

where the expression is written assuming that $t = 0$ is the instant of voltage removal, and

$$A_k = \frac{C_k V_{DC}}{\tau_k}\left(1 - e^{-t_{pol}/\tau_k}\right). \qquad (13)$$

It should be noted that the step DC voltage and the short-circuit are actually exponential transients with the duration of few tens of seconds. As we already stated in the previous section however, we are looking for long-range polarization mechanisms that manifest themselves when the source voltage is already at DC, thus the assumption of instantaneous commutation seems to be acceptable.

Equations (12) and (13) indicate that C_k and τ_k must be inferred from the depolarization current measurement. The method is illustrated with the support of Fig. 3.

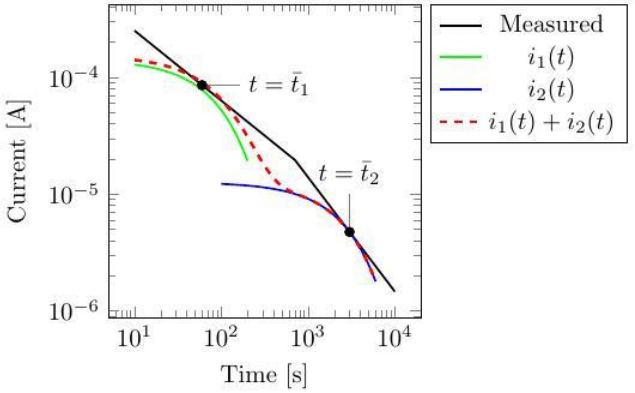

FIGURE 3. Modelling the depolarization current curve. Example with N = 2 polarization processes.

Taking the logarithm of current $i_k(t)$, defined in (12), we have:

$$I_k(t) = \ln i_k(t) = \ln A_k - \frac{t}{\tau_k} = \ln A_k - \frac{e^\xi}{\tau_k}, \qquad (14)$$

with $\xi = \ln t$. Let $i_m(t)$ be the measured depolarization current; since it is a discharge current, we can expect it to be monotonically decreasing as a function of time, therefore the derivative of $I_m(t) = \ln i_m(t)$ in a given time instant $\bar{t}_k$ can be written as

This article has been accepted for publication in a future issue of this journal, but has not been fully edited. Content may change prior to final publication. Citation information: DOI 10.1109/ACCESS.2021.3066286, IEEE Access

$$\left.\frac{dI_m}{d(\ln t)}\right|_{\bar{t}_k} = \left.\frac{dI_m}{d\xi}\right|_{\ln \bar{t}_k} = -m\,, \tag{15}$$

with $m > 0$. A simple way to derive the time constant τ_k comes from the condition

$$\left.\frac{dI_k}{d(\ln t)}\right|_{\bar{t}_k} = \left.\frac{dI_m}{d(\ln t)}\right|_{\bar{t}_k}, \tag{16}$$

which becomes, from (14) and (15):

$$\tau_k = \frac{\bar{t}_k}{m}. \tag{17}$$

The time instant $\bar{t}_k$ is arbitrary. Once the N time constants τ_k have been estimated, capacitances C_k can be determined by imposing, for each $\bar{t}_k$, the following condition:

$$i_{dep}(\bar{t}_k) = i_m(\bar{t}_k)\,. \tag{18}$$

Using (12) and (13), current $i_{dep}(\bar{t}_k)$ in (18) can be written as

$$i_{dep}(\bar{t}_k) = \sum_{j=1}^{N} A_j\, e^{-\bar{t}_k/\tau_j} = \sum_{j=1}^{N} a_{kj} C_j\,,$$

which yields the linear system

$$\begin{bmatrix} a_{11} & \cdots & a_{1N} \\ \vdots & \ddots & \vdots \\ a_{N1} & \cdots & a_{NN} \end{bmatrix} \begin{bmatrix} C_1 \\ \vdots \\ C_N \end{bmatrix} = \begin{bmatrix} i_m(\bar{t}_1) \\ \vdots \\ i_m(\bar{t}_N) \end{bmatrix}, \tag{19}$$

where

$$a_{kj} = \frac{V_{DC}}{\tau_j}\left(1 - e^{-t_{pol}/\tau_j}\right) e^{-\bar{t}_k/\tau_j}\,. \tag{20}$$

The implementation of this method is iterative. One starts to choose a time $\bar{t}_N$ which is close to the maximum measured depolarization time and computes τ_N and C_N. Then $\bar{t}_{N-1} < \bar{t}_N$ is picked in such a way that $i_{dep}(t)$ approximates the measured current; note that C_N and C_{N-1} are computed by solving (19), so the value of C_N changes from the initial step. The process is iterated until time instants $\bar{t}_1, \ldots, \bar{t}_N$ are got and the total depolarization current $i_{dep}(t)$ is a good approximation of the measured one. Some remarks have to be made:

- the method is empirical, but the advantage is that only time instants $\bar{t}_k$ are empirically selected;
- this method can fit the measured current with relatively few time constants, which means that the main polarization processes can be successfully identified: this is much better than what is usually achieved with simpler interpolation methods [20,21,22], which require a great number of time constants that have not any physical meaning;
- as demonstrated in the following very good fittings can be obtained with the proposed method, but the outcome may also be used to perform a non-linear least squares optimization that helps improving the quality of the result [23].

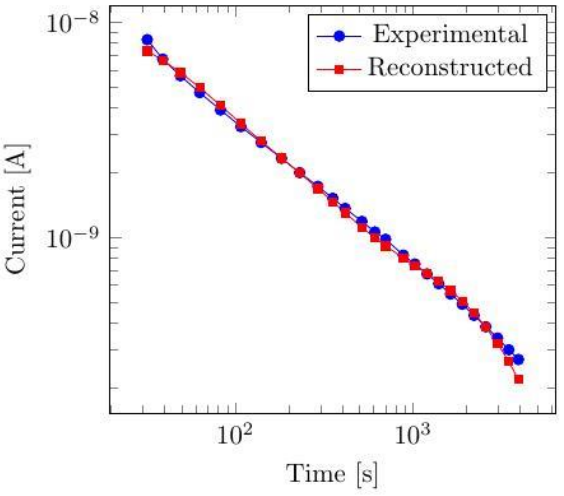

FIGURE 4. Depolarization current fitting by the proposed algorithm to experimental data measured in [24].

An experimental depolarization current, measured in [24], from a paper-oil sample is fitted in Fig. 4, to show the effectiveness of the method. The experiment was performed at $V_{DC} = 24$ kV, on a specimen with $d = 0.8$ mm and $A = 120 \times 60$ mm^2. In Table I the fitting parameters are summarized. It is worth noting that the highest susceptivity is χ_3, which is the one associated to the longest time constant: indeed, greater dipoles (hence electric permittivities) are associated to the slower polarization mechanisms, such as Maxwell-Wagner-Sillars polarization, or electrode polarization [12].

TABLE I
FITTING PARAMETERS

k	$\bar{t}_k$ [s]	τ_k [s]	C_k [F]	χ_k
1	40	38.560	$1.3130 \cdot 10^{-11}$	0.16447
2	200	192.80	$2.5441 \cdot 10^{-11}$	0.31926
3	2500	2410.0	$1.1616 \cdot 10^{-10}$	1.4577

Fitting parameter values for the experimental depolarization current measured in [24].

To verify the validity of the model presented in Fig. 1 we should be able to describe the experimental polarization current using the parameters in Table I. Resistance R is obtained from the experimental steady-state polarization current $I_{pol,\infty}$,

$$R = \frac{V_{DC}}{I_{pol,\infty}} \simeq 1.0900 \cdot 10^{13}\ \Omega\,. \tag{21}$$

This article has been accepted for publication in a future issue of this journal, but has not been fully edited. Content may change prior to final publication. Citation information: DOI 10.1109/ACCESS.2021.3066286, IEEE Access

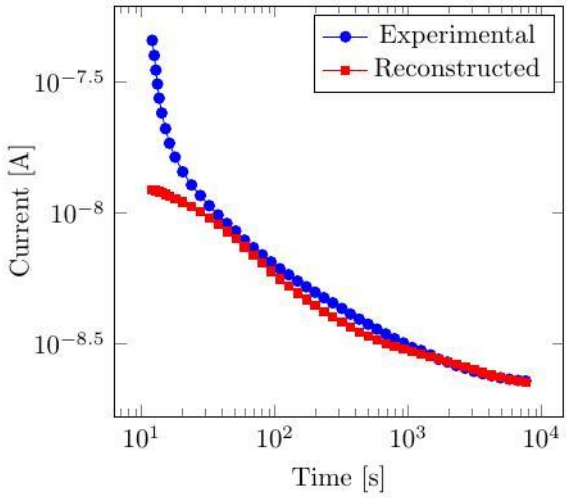

FIGURE 5. Fitting of the proposed model to the measured polarization current from [24].

The fitting of the proposed model to the measured polarization current from [24] is shown in Fig. 5. The initial transient cannot be modelled properly because experimental data in the first 10 seconds are not available [24], but for longer times the fitting is very good.

IV. SIMULATIONS AND DISCUSSION

In this section we show that polarization processes in the differential model can impact the transient simulation of a typical HVDC paper-insulated cable, whose parameters are given in Table II. The details of the numerical implementation will be given in a separate article [25].

TABLE II
CABLE PARAMETERS

Rated voltage	$V_n = 250$ kV
Rated current	$I_n = 1$ kA
Conductor radius	$r_c = 23$ mm
Insulation thickness	$d_{ins} = 20$ mm

Cable parameters used in the simulations.

The insulating material is that discussed in the previous section. From the experimental data in [24] it comes out that $\varepsilon_\infty = 4\varepsilon_0$. Paper measurements in [24] are performed only at room temperature, $T_{ref} = 20°\text{C}$, thus for the temperature coefficient in (8) we use a typical value for paper from [16], $\alpha = 1.05 \times 10^4$ K. The average insulation electric field, from the cable parameters in Table II, is $V_n/d_{ins} = 12.5$ kV/mm. This field is sufficiently small, and oil-paper conductivity is large enough, to be able to neglect the dependence of conductivity on field [2]. In conclusion, the expression of the conductivity adopted in the simulations is:

$$\sigma(T) = \sigma_0 \exp\left[-\alpha\left(\frac{1}{T + 273.15} - \frac{1}{T_{ref} + 273.15}\right)\right], \qquad (22)$$

with $\sigma_0 = d \,/\, (A \cdot R) \simeq 1.0194 \times 10^{-14}$ S/m. In general capacitances C_k and time constants τ_k may be temperature-dependent too, but without measurements at temperatures other than T_{ref} we must consider them constant. The external temperature is fixed at 20°C, while different internal temperatures are evaluated (30°C, 40°C and 50°C), corresponding to different loading conditions.

The cable is supplied by the voltage waveform depicted in Fig. 6. Field behavior during energization, inversion and discharge transients is simulated. To simulate realistic switching, the voltage jumps in Fig. 5 are implemented by an exponential law, i.e.

$$\Delta V \, e^{-(t-t_0)/\tau_g}, \qquad (22)$$

where $\tau_g = 0.5\,s$ and $\Delta V = +V_n, -2V_n, +V_n$ in the three switching times $t_0 = 0, 5 \cdot 10^4, 10^5$ [s].

The insulation electric field profiles at different instants are shown in Figs. 6 to 9, to highlight the differences between the "improved" model (9) and the "standard" one (2).

Fig. 7 shows the resistive steady-state field at the end of the energization transient. The two models predict the same profile because the steady-state field is determined only by the electric conductivity σ and the cable geometry.

Figs. 8, 9 and 10 show the electric field profiles in the three simulated transients. In all cases, one can expect that the transient predicted by the improved model is slower than the one predicted by the standard model: this is due to the polarization processes that are considered by (9).

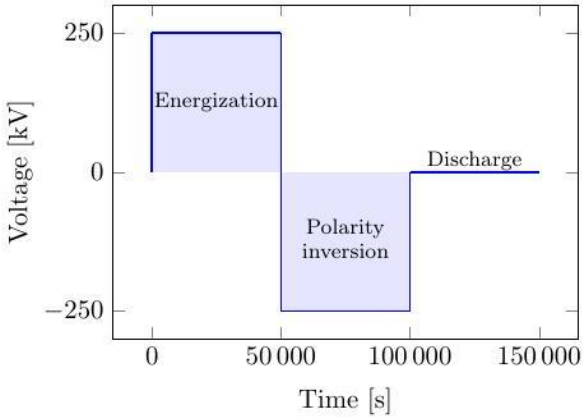

FIGURE 6. Voltage supply waveform used in the simulations.

This article has been accepted for publication in a future issue of this journal, but has not been fully edited. Content may change prior to final publication. Citation information: DOI 10.1109/ACCESS.2021.3066286, IEEE Access

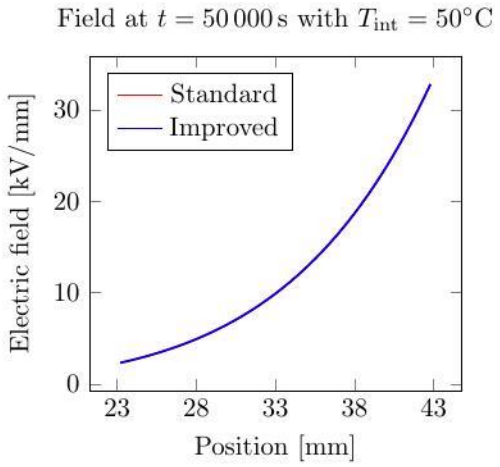

FIGURE 7. Steady-state electric fields of the energization transient.

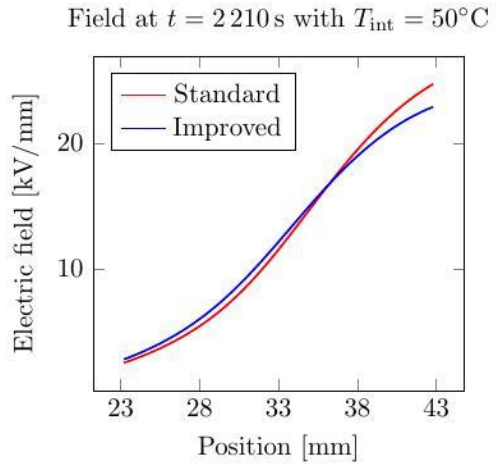

FIGURE 8. Transient electric fields during energizations.

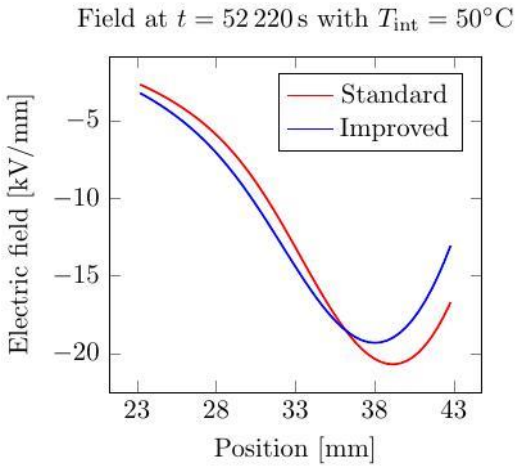

FIGURE 9. Transient electric fields during polarity inversion.

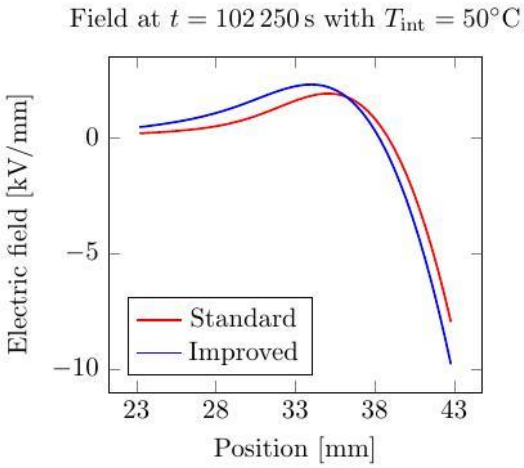

FIGURE 10. Transient electric fields during discharge.

To summarize, let

$$\Delta E(x,t) = \frac{E_{imp}(x,t) - E_{std}(x,t)}{E_{avg}} \tag{23}$$

be the difference between the electric field obtained with the improved (E_{imp}) and standard (E_{std}) models as a function of radial position and time, divided by the average electric field, $E_{avg} = 12.5\ \mathrm{kV/mm}$. The maximum amplitude of $\Delta E(x,t)$ is depicted in Fig. 11 for each time instant,

$$\delta_E(t) = \max_{x\in[r_c, r_c+d_{ins}]} |\Delta E(x,t)|\,. \tag{24}$$

The figure shows $\delta_E(t)$ at various temperature drops $\Delta T = T_{int} - T_{ext}$, with $T_{ext} = 20°\mathrm{C}$. As can be seen, its values increase with temperature. Moreover, during the inversion transient $\delta_E(t)$ is approximately twice than in the energization and discharge ones: this is due to the voltage step of the commutation, which is $2V_n$ in case of polarity inversion and V_n in the other two stages.

The space and time dependence of $\Delta E(x,t)$ is summarized in Figs. 12 and 13, where the cases with $\Delta T = 10°\mathrm{C}$ and $\Delta T = 30°\mathrm{C}$ are shown, respectively.

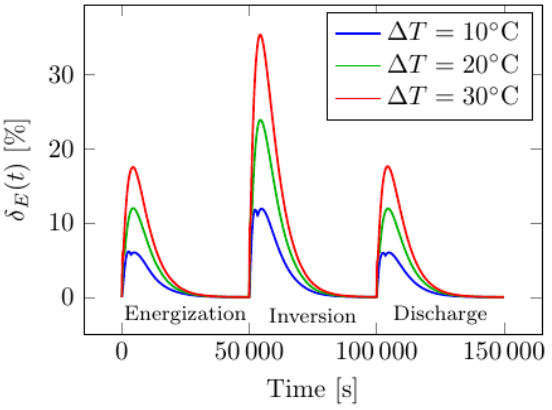

FIGURE 11. Maximum fields difference $\delta_E(t)$ between the electric field profiles at different temperature drops.

This article has been accepted for publication in a future issue of this journal, but has not been fully edited. Content may change prior to final publication. Citation information: DOI 10.1109/ACCESS.2021.3066286, IEEE Access

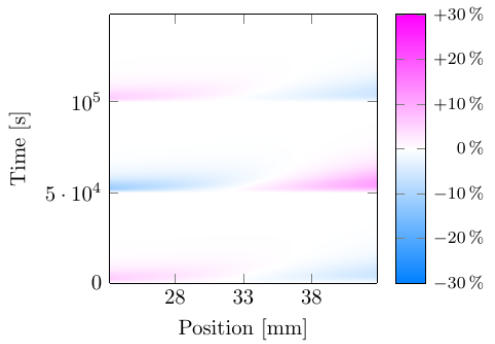

FIGURE 12. **Fields difference $\Delta E(x,t)$ with $\Delta T = 10°C$.**

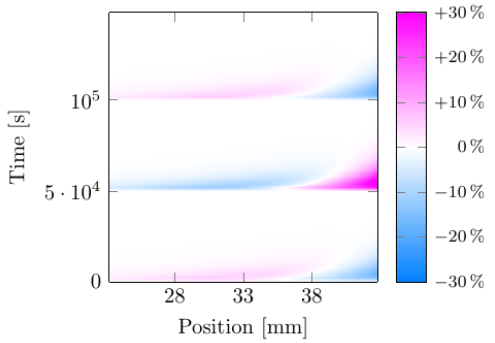

FIGURE 13. **Fields difference $\Delta E(x,t)$ with $\Delta T = 30°C$.**

In the blue regions $\Delta E < 0$, thus $E_{std} > E_{imp}$, while in the violet ones $\Delta E > 0$, which means $E_{imp} > E_{std}$. The figures show that the difference between E_{imp} and E_{std}, regardless of the sign, intensifies immediately after a commutation and it is spread all over the insulating region, not just confined in narrow areas. The colored regions in Fig. 12 are more intense than the ones in Fig. 11, meaning that ΔE becomes larger as temperature drop ΔT increases.

In the white regions $\Delta E = 0$, therefore $E_{std} = E_{imp}$. This situation is reached when both models are at steady-state and the electric field profile for both E_{std} and E_{imp} is determined by the condition

$$\nabla \cdot (\sigma \boldsymbol{E}) = 0\,, \tag{25}$$

which holds for homogeneous materials.

V. CONCLUSIONS

This article proposes an improved approach, compared to the conventional one, to model the electric field distribution in HVDC oil-paper cables during voltage transients. The novelty here is to incorporate the dynamics of dielectric polarization mechanisms into the fundamental equations and relevant simulations. A simple empirical method is proposed, which is based on a circuital model, to derive the differential model parameters from polarization and depolarization current measurements performed on appropriate insulation specimens. It is shown that the fitting of the model to experimental data can be accurate and that the most significant polarization processes under DC excitation can be successfully identified. The simulations performed on a typical paper insulated cable show that the impact of polarization dynamics on the electric field transient can be significant, in terms of both the transient duration and of its magnitude and profile across cable insulation. It is observed also that differences between the conventional model and the proposed one increase with voltage amplitude and temperature gradient. Future studies will focus on solid polymeric dielectrics, where differences with respect to the conventional model are expected to be larger.

REFERENCES

[1] G. C. Montanari, P. Morshuis, P. Seri and R. Ghosh, "Ageing and reliability of electrical insulation: the risk of hybrid AC/DC grids," *High Voltage*, vol. 5, no. 5, pp. 620-627, 2020.

[2] M. Jeroense and P. Morshuis, "Electric fields in HVDC paper-insulated cables," *IEEE Transactions on Dielectrics and Electrical Insulation*, vol. 5, no. 2, pp. 225-236, 1998.

[3] G.C. Montanari, "Notes on theoretical and practical aspects of polymeric insulation aging," *IEEE Transactions on Dielectrics and Electrical Insulation*, vol. 29, no. 4, pp. 30-40, August 2013.

[4] L. Dissado, G. Mazzanti, G.C. Montanari, "The role of trapped space charges in the electrical aging of insulating materials," *IEEE Transactions on Dielectrics and Electrical Insulation*, vol. 4, no. 5, pp. 496-506, 1997.

[5] P. Morshuis and J. Smit, "Partial discharges at DC voltage: their mechanism, detection and analysis," *IEEE Transactions on Dielectrics and Electrical Insulation*, vol. 12, no. 2, pp. 328-340, 2005.

[6] L. Niemeyer, "A generalized approach to partial discharge modeling," *IEEE Transactions on Dielectrics and Electrical Insulation*, vol. 2, no. 4, pp. 510-528, 1995.

[7] P. Das and S. Chakravorti, "Simulation of PD patterns due to a narrow void in different E-field distribution,", *Journal of Electrostatics*, vol. 68, no. 3, pp. 218-226, 2010.

[8] Evaluation and qualification of electrical insulation systems, IEC 60505 (2011).

[9] G. C. Montanari, P. Seri and R. Ghosh, "DC Voltage supply in T&D: what about electrical insulation reliability and maintenance?," in *2020 IEEE/PES Transmission and Distribution Conference and Exposition (T&D)*, pp. 1-5, Chicago, IL, 2020.

[10] S. J. Frobin, C. Freye, C. F. Niedik and F. Jenau, "Generic field simulation framework for HVDC cables," in *IEEE 2nd International Conference on Dielectrics*, Budapest, Hungary, 2018.

[11] C. Jörgens, F. Kasolis and M. Clemens, "Numerical simulations of temperature stability limits in High-Voltage Direct Current cable insulations," *IEEE Transactions on Magnetics*, vol. 55, no. 6, pp. 1-4, 2019.

[12] A. K. Jonscher, Dielectric relaxation in solids, Chelsea Dielectric Press Ltd, London, 1983.

[13] G. C. Montanari, P. Seri and H. Naderiallaf, "A contribution to everlasting electrical insulation for DC voltage: PD-phobic materials", in *IEEE Access*, vol. 8, pp. 41882-41888, 2020.
[14] B. Du, C. Han, Z. Li and J. Li, "Improved DC conductivity and space charge characteristics of XLPE for HVDC cable application: effect of voltage stabilizers," in *IEEE Access*, vol. 7, pp. 66576-66583, 2019.
[15] G. C. Montanari, R. Hebner, P. Morshuis and P. Seri, "An approach to insulation condition monitoring and life assessment in emerging electrical environments," *IEEE Transactions on Power Delivery*, vol. 34, no. 4, pp. 1357-1364, 2019.
[16] E. Occhini and G. Maschio, "Electrical characteristics of oil-impregnated paper as insulation for HV DC cables," *IEEE Transactions on Power Apparatus and Systems*, Vols. PAS-86, no. 3, pp. 312-326, 1967.
[17] L.A. Dissado and J.C. Fothergill, Electrical Degradation and Breakdown in Polymers, P. Peregrinus Press, 1992.
[18] G.C. Montanari, G. Mazzanti, F. Palmieri, A. Motori, G. Perego and S. Serra, "Space charge trapping and conduction in LDPE, HDPE and XLPE," *Journal of Phys. D: Appl. Physics*, vol. 34, pp. 2902-2911, 2001.
[19] G.C. Montanari, "The electrical degradation threshold of polyethylene investigated by space charge and conduction current measurements," *IEEE Transactions on Dielectrics and Electrical Insulation*, vol. 7, no.3, pp. 309-315, 2000.
[20] V. der Houhanessian and W.S. Zaengl, "On-site diagnosis of power transformers by means of relaxation current measurements," Conference Record of the *1998 IEEE International Symposium on Electrical Insulation*, Arlington, VA, USA, 1998, vol.1, pp. 28-34.
[21] V. der Houhanessian and W.S. Zangl, "Time domain measurements of dielectric response in oil-paper insulation systems," Conference Record of the *1996 IEEE International Symposium on Electrical Insulation*, Montreal, Quebec, Canada, 1996, vol. 1, pp.47-52.
[22] V. der Houhanessian, "Measurement and analysis of dielectric response in oil-paper insulation systems," Ph.D. dissertation, ETH Zürich, Zürich, 1998.
[23] P. Cambareri, C. de Falco, L. Di Rienzo, P. Seri and G. C. Montanari, "Simulation of transient electric fields in HVDC insulation systems based on polarization current measurements and modelling," submitted to *XXII International Symposium on High Voltage Engineering*, 2021.
[24] R. Wiengarten, F. Jenau and B. Bakija, "Polarization and depolarization behavior of various oil impregnated paper insulations stressed by very high DC field strength," in *XVII International Symposium on High Voltage Engineering*, Hannover, Germany, 2011.
[25] P. Cambareri, C. de Falco, L. Di Rienzo, P. Seri and G. C. Montanari, "Finite difference and equivalent circuit modeling of polarization in HVDC cables," in preparation.

Pasquale Cambareri was born in Busto Arsizio, Italy, in August 1992. He received the M.Sc. Degree in Electrical Engineering from Politecnico di Milano in 2019. Since November 2019, he has been a Ph.D. student in Electrical Engineering at Dipartimento di Elettronica, Informazione e Bioingegneria (DEIB), Politecnico di Milano. His work focuses on the multi-physics numerical modeling of HVDC cables.

Carlo de Falco received the M.Sc. degree in Electrical Engineering from Politecnico di Milano in 2002 and a Ph.D. in Applied Mathematics from Università Statale di Milano in 2006. After holding research and teaching positions at Bergische Universität Wuppertal and Dublin City University, he joined, since 2009, Politecnico di Milano where he is currently Associate Professor of Numerical Analysis with the Modelling and Scientific Computing (MOX) Laboratory of the Department of Mathematics. His research is mainly focused on numerical methods for solving Partial Differential Equations with applications in Electronics, Electrical Engineering, Fluid Dynamics and Material Science.

Luca Di Rienzo (Senior Member, IEEE) received the Laurea (M.Sc.) (cum laude) and Ph.D. degrees in electrical engineering from the Politecnico di Milano, in 1996 and 2001, respectively, and the B.S. degree (cum laude) in mathematics from Università Statale di Milano, in 2020. He is currently an Associate Professor with the Dipartimento di Elettronica, Informazione e Bioingegneria, Politecnico di Milano. His research interests are in the field of computational electromagnetics. He is a member of the editorial board of *COMPEL - The International Journal for Computation and Mathematics in Electrical and Electronic Engineering* and *Sensing and Imaging* and an associate editor-in-chief of *The Applied Computational Electromagnetics Society Journal*.

Paolo Seri was born in Macerata, Italy, on June, 4th 1986. He received the M.Sc. degree in energy engineering in 2012 and PhD in electrical engineering in 2016, both from the University of Bologna. From 2017 he is part of the Laboratory of Innovative Materials for Electrical Systems (LIMES) of the University of Bologna as a research fellow, currently working on the topics of HVDC cables design, partial discharge detection and modelling, and characterization of dielectric materials. He is also Assistant

Professor at the Department of Electrical, Electronic and Information Engineering, DEI, of Bologna University.

Gian Carlo Montanari (M'87, SM'90, F'00) is currently Research Faculty III at the Center for Advanced Power Systems (CAPS) of the Florida State University, USA, and Alma Mater professor at the Bologna University, Italy. He has been Full Professor of Electrical Technology at the Department of Electrical, Electronic and Information Engineering of the University of Bologna, teaching courses on Technology, Reliability and Asset Management. He has worked since 1979 in the field of aging and endurance of insulating materials and systems, diagnostics of electrical systems, asset management and innovative electrical materials (magnetics, electrets, super-conductors, nano-materials). He has been engaged also in the fields of power quality and energy market, power electronics, reliability and statistics of electrical systems, and smart grid. He has been recognized with several awards, including the IEEE Ziu-Yeda, Thomas W. Dakin, Whitehead, Eric Forster and IEC 1906 awards. He was founder and President of the spin-off Techimp, established in 1999. He is author or co-author of more than 800 scientific papers.